Electrodeposition of Pt onto RuO_2(110) Single-Crystal Surface

Miomir B. Vukmirovic,* Ping Liu, James T. Muckerman, and Radoslav R. Adzic

Chemistry Department, Brookhaven National Laboratory, Upton, New York 11973

Received: June 1, 2007; In Final Form: July 26, 2007

The electrodeposition of Pt on RuO_2(110) from acid solutions of several Pt complexes was studied using programmed potential step or potential sweep methods. The RuO_2(110) single-crystal surface was obtained by gas-phase oxidation of Ru(0001). The electrodeposition process is characterized by a large crystallization overpotential and three-dimensional growth from a Pt adlayer. The mismatch between the RuO_2(110) and Pt lattices is the likely origin of that overpotential. The nucleation is instantaneous, as verified by potential step experiments. The process starts with depositing a 0.25 ML of Pt, with Pt atoms arranged in a c(2 × 2) array, which is followed by the growth of Pt islands and three-dimensional clusters as in the Stranski−Krastanov growth mode. Density functional theory calculations were used to help in elucidating atomically resolved electrochemical scanning tunneling microscopy (ECSTM) images of the initial stages of Pt deposition. A Pt adlayer on RuO_2(110) has lower catalytic activity for the oxygen reduction reaction compared to Pt, which is in agreement with a large calculated upshift of the d-band center of a low-coverage Pt deposit on RuO_2-(110) as well as a lack of the oxygen adsorption in a bridge configuration on that surface.

1. Introduction

There are only a handful of studies of metal electrodeposition on conductive metal oxide surfaces. Likewise, the catalytic properties of electrodeposited metal/metal oxide systems are largely unexplored. These systems have a considerable potential as electrocatalysts, despite some restrictions that the electrochemical media can impose. Platinum monolayer/multilayer deposits on metal oxides are candidate electrocatalysts for improving the oxygen reduction reaction (ORR) due to the plausible effects of the oxide's OH or O and vacancy sites on the OH coverage on Pt and possible enhanced splitting of the O−O bond.[1] Furthermore, increased stability of the Pt deposits on oxide surfaces may result from adsorption of Pt cations on oxide surfaces.[2] Beside the above features, an appropriate metal oxide support must be stable under the oxidizing conditions of oxygen reduction and preferably conductive.

We selected the RuO_2(110) surface as a model system because of its rare suitability for atomic-scale surface chemistry and its conductivity and stability under the oxidizing conditions of an oxygen cathode. The electrodeposition of metals on compound substrates (metal oxides, chalcogenides, carbides, etc.) differs considerably from that on foreign metal substrates since usually at least two chemically different kinds of atomic sites are available on the surface of compound substrates. The RuO_2 possesses metallic conductivity[3] due to ruthenium d-electrons.[4] The only work on electrodeposition of metals on RuO_2 is apparently the study of Ag electrodeposition by Hepel et al.[5,6]

The objective of this work is to obtain basic information on the initial phases of Pt monolayer-level deposition on Ru oxide surfaces. Such information would be valuable for elucidating the initial phases of metal growth on metal oxide surfaces under electrochemical conditions. In addition, the catalytic properties of such surfaces could be determined and the potential for electrocatalysis estimated. Electrochemical experiments showed that Pt deposition involves large crystallization overpotential. A deposition of a 0.25 ML of Pt (Pt coverage was calculated in relation to Ru atoms), with Pt atoms arranged in a c(2 × 2) array, is followed by Pt island growth. Density functional theory (DFT) is used to calculate deposits of various Pt coverages and to compare them with atomically resolved electrochemical scanning tunneling microscopy (ECSTM) images of the initial stages of Pt deposition on RuO_2(110).

2. Experimental Section

The RuO_2(110) single-crystal surface was obtained by gas-phase oxidation of Ru(0001).[7] A disk-shaped Ru(0001) single crystal, 8 mm in diameter and 2 mm thick, was obtained from Metal Crystal and Oxides, Cambridge, England. It was mechanically polished with 1 μm diamond paste. After the cleaning procedure, the crystal was placed inside a quartz tube. Inductive heating in a stream of a mixture of Ar and ∼100 ppm O_2 gas produced chemical oxidation. The oxide was formed in samples held for about 2 min at temperatures between 600 and 800 K. From the flow rate of the gas mixture we estimated that the O_2 pressure in the quartz tube was around 0.1 mbar. The sample was transferred to the electrochemical cell protected with a droplet of sulfuric acid. This procedure yields a well-ordered RuO_2(110) single-crystal surface, which was verified by atomically resolved images obtained by ECSTM. The ECSTM images were obtained in 50 mM H_2SO_4 at open circuit potential (OCP). Voltammetry curves obtained from such surfaces confirmed that they were well ordered, being similar to those obtained for ordered bulk RuO_2(110). The in situ scanning tunneling microscopy (STM) studies were performed using a Molecular Imaging Pico STM with a 300S scanner and a 300S Pico Bipotentiostat. The tunneling tips were made of a polycrystalline Pt−20% Ir wire and coated with Apiezon wax. The platinum wires served as the reference and counter electrodes in ECSTM experiments. The voltammetry experiments were carried out in a standard three-electrode electrochemical cell with a Ag/AgCl/KCl (3 M) reference electrode and a Pt foil counter electrode. All the potentials in the text are reported versus a reversible

* Corresponding author. E-mail: miomir@bnl.gov. Fax: 631-344-5815.

10.1021/jp0742719 CCC: $37.00
Published on Web 10/03/2007

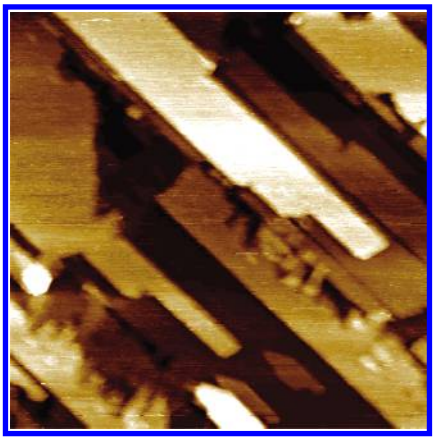

Figure 1. ECSTM image of the RuO_2(110) oxide obtained by chemical oxidation of Ru(0001). Image obtained in 50 mM H_2SO_4 at open circuit condition (0.95 V); size 200 nm × 200 nm, *Z* range 1 nm.

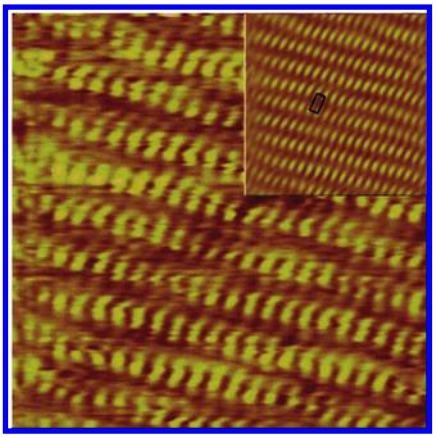

Figure 2. Atomically resolved ECSTM image of RuO_2 stripes (and its Fourier transform shown in the inset) obtained in 50 mM H_2SO_4 at open circuit condition (0.95 V); size 5.8 nm × 5.8 nm.

hydrogen electrode (RHE). Pt was deposited by programmed potential pulses or potential sweeps from K_2PtCl_4 or $K_2Pt(NO_2)_4$ dissolved in 50 mM H_2SO_4 or 10 mM HCl. Concentrations of Pt salts range from 10^{-6} to 10^{-3} M. All the solutions were made with high-purity grade chemicals and Millipore Q UV plus water.

3. Results and Discussion

3.1. Synthesis and Characterization of RuO_2(110) Single-Crystal Surface. The oxidation of the Ru(0001) surface was preformed in a stream of Ar containing about 100 ppm O_2 at temperatures between 600 and 800 K. The ECSTM image of such a surface is given in Figure 1. To prevent surface contamination, the oxidized Ru surface was examined in 50 mM H_2SO_4 under open circuit conditions (~0.95 V). Figure 1 shows that oxide grows as long parallel stripes. The step height of these stripes is about 3 Å, corresponding to one monolayer of Ru oxide. The covering of the surface by oxide was examined by probing the surface in several places by ECSTM. In each of them the surface was completely covered with oxide suggesting that the whole surface was covered by oxide. Additional evidence comes from voltammetry, which is discussed in the following section. Atomically resolved ECSTM pictures unveil the nature of the oxide stripes, Figure 2. The structure of the oxide stripes displays a rectangular 6.3 Å × 3.1 Å unit cell. Within the limits of accuracy of the ECSTM technique, this unit cell corresponds to the rutile structure of RuO_2 with the (110) orientation (6.38 Å × 3.11 Å).[8] Similar rectangular stripes

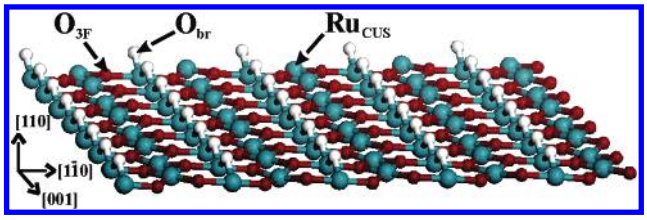

Figure 3. Model of RuO_2(110) surface in perspective view.

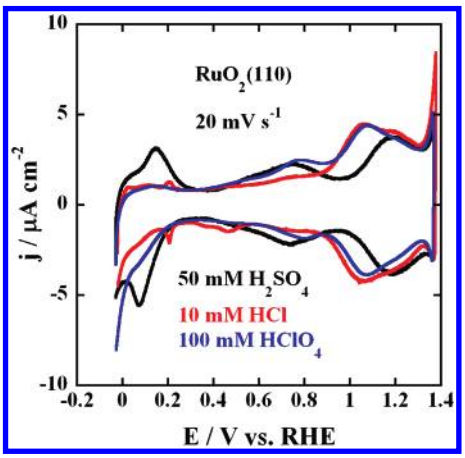

Figure 4. Voltammetry curves of a RuO_2(110) surface in deoxygenated 50 mM H_2SO_4, 10 mM HCl, and 100 mM $HClO_4$.

and internal structures with the same unit cell were observed in images from the ultrahigh vacuum (UHV) gas-phase oxidation of Ru(0001) with high doses of O_2 at 600−800 K.[9] Low-energy electron diffraction (LEED) and STM data showed that this is a RuO_2(110) oxide film, growing epitaxially on the Ru(0001) surface as an incommensurate layer.[9,10] The misfit between RuO_2(110) with cell dimensions of 6.38 Å × 3.11 Å and the nonprimitive rectangular cell for Ru(0001) with cell dimensions of 4.70 Å × 2.70 Å is too large to expect a pseudomorphic growth of oxide. This incommensuration between Ru and RuO_2 suggests that the oxide film is not strained.

A ball-and-stick model of the RuO_2(110) surface is shown in Figure 3. The RuO_2(110) surface contains two kinds of coordinatively unsaturated (CUS) atoms: twofold bridging O (O_{br}) and fivefold Ru (Ru_{CUS}). The O_{3F} sites are O atoms that lie in the plane of the Ru atoms and possess its bulklike threefold coordination. The interpretation of atomically resolved ECSTM images of oxides is difficult because of strong variations in the local electronic structure, as well as geometric effects. UHV experiments of O and CO adsorption on a RuO_2(110) surface as well as its partial reduction by CO, together with DFT calculations,[9,10] showed that bright rows should be interpreted in terms of rows of bridging oxygen.

3.2. Voltammetry of RuO_2(110) Surface in Sulfuric, Perchloric, and Hydrochloric Acids. Polarization curves of a RuO_2(110) surface in deoxygenated sulfuric, perchloric, and hydrochloric acids are shown in Figure 4. The curve in sulfuric acid is very similar to that obtained for bulk (naturally grown) RuO_2.[11−13] In the case of hydrochloric acid, a comparison with the curve in ref 14 is precluded by vastly different potential limits in the two experiments. The voltammetric curve for RuO_2(110) in perchloric acid exhibits much better resolved features, yet qualitatively it does not differ substantially from those for polycrystalline samples.[15] The symmetrical shape of the polarization curves suggests reversible surface redox processes of RuO_2 in the potential range between H_2 and O_2 evolution. These surface redox processes apparently involve a change of the oxidation state of Ru and proton transfer through

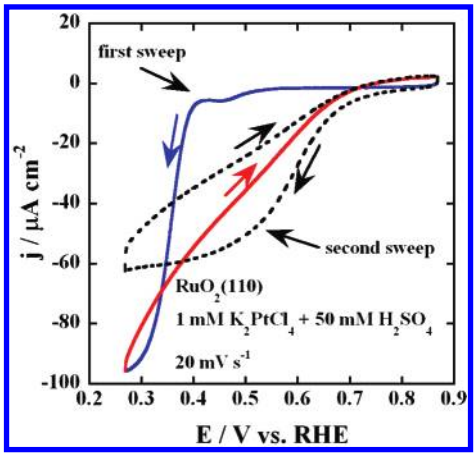

Figure 5. Voltammetry curves for the first and second sweep of Pt deposition on $RuO_2(110)$ obtained from 1 mM K_2PtCl_4 + 50 mM H_2SO_4.

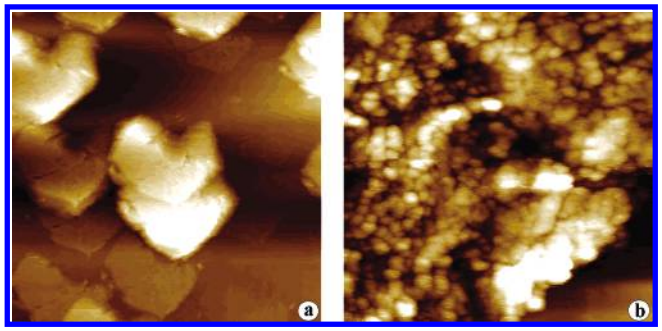

Figure 6. ECSTM images of the rectangularly shaped multilayer deposit of Pt on $RuO_2(110)$ obtained in 50 mM H_2SO_4 at open circuit condition (0.95 V). (a) 1250 nm × 1250 nm, *Z* range 100 nm. (b) Zoom of (a) 80 nm × 80 nm, *Z* range 5 nm.

conversion of O^{2-} ions to OH^- in order to maintain a charge balance. The differences among the polarization curves obtained in sulfuric, perchloric, and hydrochloric acids reflect the specific influence of the corresponding anions on the surface redox processes. The absence of characteristic Ru peaks is an indication that the Ru surface is fully covered with RuO_2.

3.3. Electrochemical Deposition of Pt onto $RuO_2(110)$. Figure 5 shows a cyclic voltammogram for the electrodeposition of Pt on $RuO_2(110)$ in 1 mM K_2PtCl_4 + 50 mM H_2SO_4 at a scan rate of 20 mV s^{-1}. The process is characterized by a large overpotential causing the appearance of the so-called "nucleation loop" that makes the current in the anodic sweep larger than the current in the cathodic sweep. This type of the current loop in the cyclic voltammogram appears associated with the nucleation and growth processes and is due to an easier nucleation on a partially Pt-covered RuO_2 surface (anodic in comparison with cathodic sweep). In addition, the real surface area of the Pt deposit is larger in the anodic sweep and it can support a larger current. The deposition starts at an overpotential of about 0.3 V (equilibrium potential is 0.642 V). There is one likely reason for the large overpotential, viz., the mismatch between the $RuO_2(110)$ and Pt lattices. An IR drop due to resistivity of RuO_2 cannot be the reason for the large overpotential because RuO_2 possesses metallic conductivity.[3] Further support for the above analysis comes from the second sweep, Figure 5, which shows that there is no overpotential for Pt deposition on Pt islands.

Figures 6−8 show a multilayer deposition of Pt on $RuO_2(110)$ obtained under various conditions. Figure 6 shows a rectangularly shaped layered deposit. It was obtained from 1 mM K_2PtCl_4 + 10 mM HCl by stepping the potential from OCP

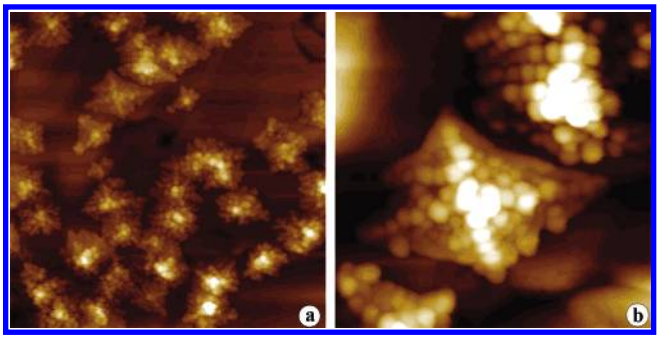

Figure 7. ECSTM images of the pyramidal multilayer deposit of Pt on $RuO_2(110)$ obtained in 50 mM H_2SO_4 at open circuit condition (0.95 V). (a) 250 nm × 250 nm, *Z* range 18 nm. (b) Zoom of (a) 70 nm × 70 nm, *Z* range 11 nm.

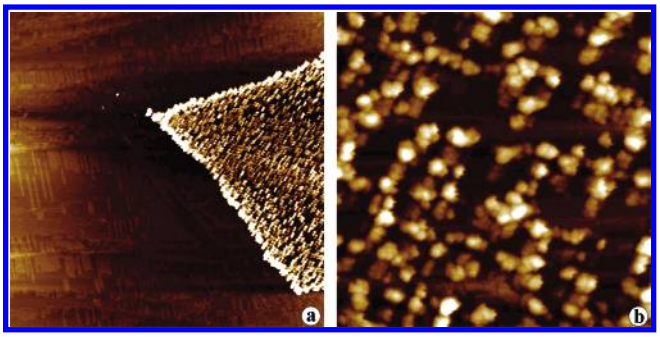

Figure 8. ECSTM images of the columnar multilayer deposit of Pt on $RuO_2(110)$ obtained in 50 mM H_2SO_4 at open circuit condition (0.95 V). (a) 800 nm × 800 nm, *Z* range 6 nm. (b) Zoom of (a) 100 nm × 100 nm, *Z* range 6 nm.

to 0.268 V until 1750 μC of total charge was passed. The size of these structures is as large as 410 nm × 360 nm × 56 nm. One can see that rectangularly shaped layered deposits grow along two orthogonal directions of RuO_2 and thus sometimes make L-shaped structures. The pyramidal deposit shown in Figure 7 was obtained from 0.1 mM K_2PtCl_4 + 10 mM HCl in eight sweeps between 0.87 and 0.02 V. The surface is covered with rectangular-based pyramids with their sides oriented along two orthogonal directions of RuO_2. Some of them stand alone, but others merged into a larger deposit. The side of the pyramid could be as large as 35 nm and the height about 8 nm. Figure 8 shows a columnar deposit. It was obtained from 10^{-3} mM K_2PtCl_4 + 50 mM H_2SO_4 by stepping the potential from OCP to 0.22 V and keeping it at that potential for 2 h. The columns are about 5 nm in height, and their base is about 9 nm in diameter, which usually consists of several Pt islands. The common features of Pt deposition in Figures 6−8 are (i) three-dimensional growth, (ii) nonuniform coverage, and (iii) three-dimensional deposit consisting of Pt islands of 2−3 nm in diameter. A three-dimensional growth could be expected for Pt deposition on $RuO_2(110)$ because of the high surface energy of Pt (2.691 J m^{-2})[16] compared to $RuO_2(110)$ (1.136 J m^{-2}).[17] Hepel et al.[5,6] report similar properties of Ag deposition on RuO_2 under similar growth conditions to ours.

The potential step deposition was used to obtain information on the mechanism of electrochemical deposition of Pt onto $RuO_2(110)$. The current transient following a potential step, in 10 mM K_2PtCl_4 + 50 mM H_2SO_4, is presented in Figure 9a. The potential was stepped from open circuit to 0.068 V, just before hydrogen evolution. To determine the type of the nucleation process involved in Pt deposition, we compared the experimental plot of the dimensionless ratio I^2/I_m^2 versus t/t_m, with the theoretical curves for instantaneous and progressive nucleation processes under diffusion control (Figure 9b).[18] *I* and

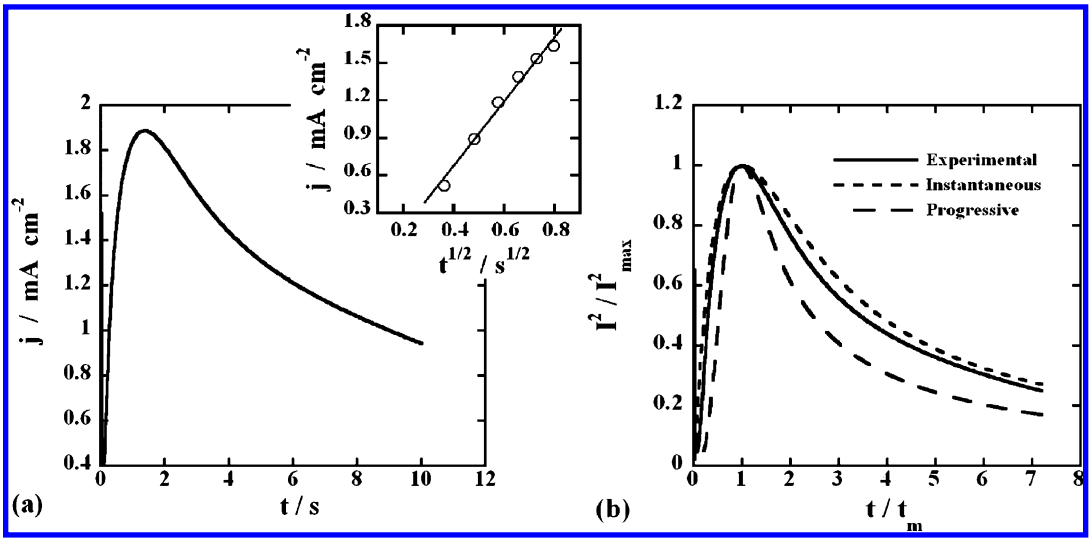

Figure 9. (a) Potentiostatic current transient for Pt deposition on RuO_2(110) obtained from 10 mM K_2PtCl_4 + 50 mM H_2SO_4 by the potential step from OCP to 0.068 V. Inset shows the plot of j vs $t^{1/2}$ obtained from the rising part of the j vs t plot. (b) Dimensionless $I^2 = I_{max}^2$ vs t/t_m experimental plot of the data in (a) compared with theoretical curves for instantaneous and progressive nucleation processes given by eqs 1 and 2, respectively.

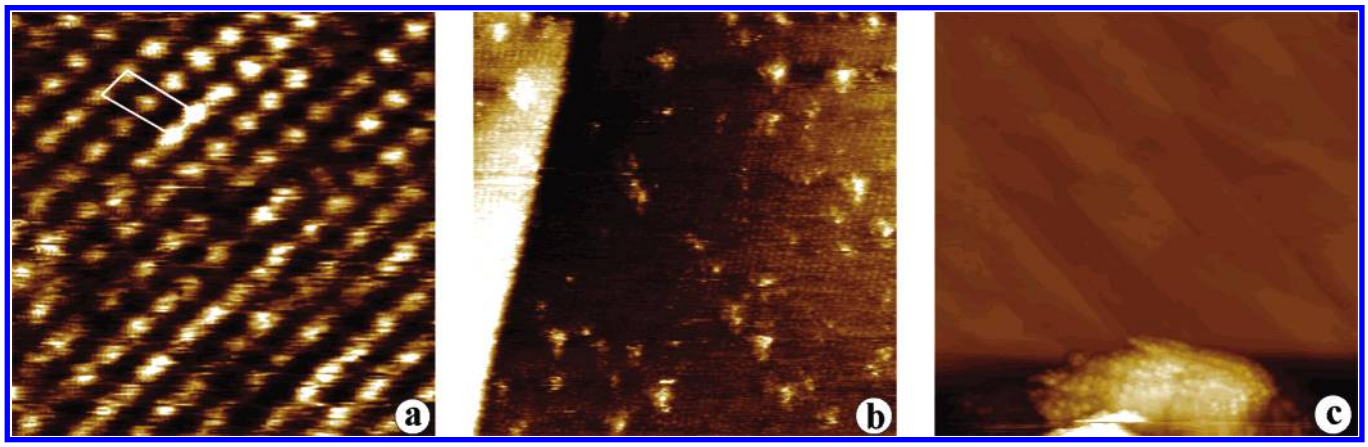

Figure 10. ECSTM images of the evolution of Pt deposit on RuO_2(110) with increasing amount of Pt (see text for details). They are obtained in 50 mM H_2SO_4 at open circuit condition (0.95 V). (a) 3.9 nm × 3.9 nm. (b) 24 nm × 24 nm. (c) 200 nm × 200 nm, Z range 25 nm.

I_m are the current and the current at maximum, respectively, while t and t_m are the corresponding times. Expressions for theoretical curves for the instantaneous and progressive nucleation processes are, respectively,

$$\frac{I^2}{I_m^2} = \frac{1.9542}{t/t_m}\{1 - \exp[-1.2564(t/t_m)]\}^2 \qquad (1)$$

and

$$\frac{I^2}{I_m^2} = \frac{1.2254}{t/t_m}\{1 - \exp[-2.3367(t/t_m)^2]\}^2 \qquad (2)$$

They show that the dimensionless plot is in good agreement with an instantaneous nucleation process, especially the rising part of the curve which demonstrates a clear linear dependence of j versus $t^{1/2}$ (see the inset of Figure 9a).

3.4. Initial Stage of Electrochemical Deposition of Pt onto RuO_2(110). Figure 10 shows a series of ECSTM pictures describing evolution of Pt deposit with increasing amount of deposited Pt. Figure 10, parts a and b, shows atomically resolved ECSTM images of the oxide stripes after Pt deposition from 1 mM K_2PtCl_4 + 50 mM H_2SO_4 by stepping the potential from OCP to 0.268 V and holding it at that potential until 50 and 80 μC of total charge was passed, respectively. Figure 10a consists of bright spots in a rectangular-centered arrangement (5.8 Å × 12.7 Å), while on Figure 10b, besides bright spots arranged in rectangular-centered array one can see small mounds and RuO_2(110) step. Figure 10c depicts the Pt deposit obtained under same conditions as for the Pt deposit shown in Figure 10, parts a and b, except that total charge that was passed was 1000 μC. That picture reveals a three-dimensional deposit consisting of small Pt islands similar to Pt deposits described in the previous section. In order to better understand atomically resolved ECSTM pictures, DFT calculations[19] were conducted to obtain the geometries and electronic structures of Pt adsorption on the stoichiometric RuO_2(110) surface at different coverages.

DFT calculations of Pt adsorption on the RuO_2(110) surface were performed using the CASTEP code.[20] Ultrasoft pseudopotentials expanded in a plane-wave basis in reciprocal space were employed (340 eV cutoff),[21] and the RPBE gradient-corrected exchange-correlation functional was used.[22] RuO_2(110) surfaces were modeled by a two-layer slab geometry (two O−Ru_2O_2−O units, hence six atomic layers) with a vacuum of 11 Å between the slabs. Upon increasing the number of layers to four, the changes in the relative energies for Pt adsorption at the different sites, which are our interest here, were negligible (less than 0.05 eV). The outermost surface layer was allowed to fully relax with the adsorbates. Brillouin zone sampling was

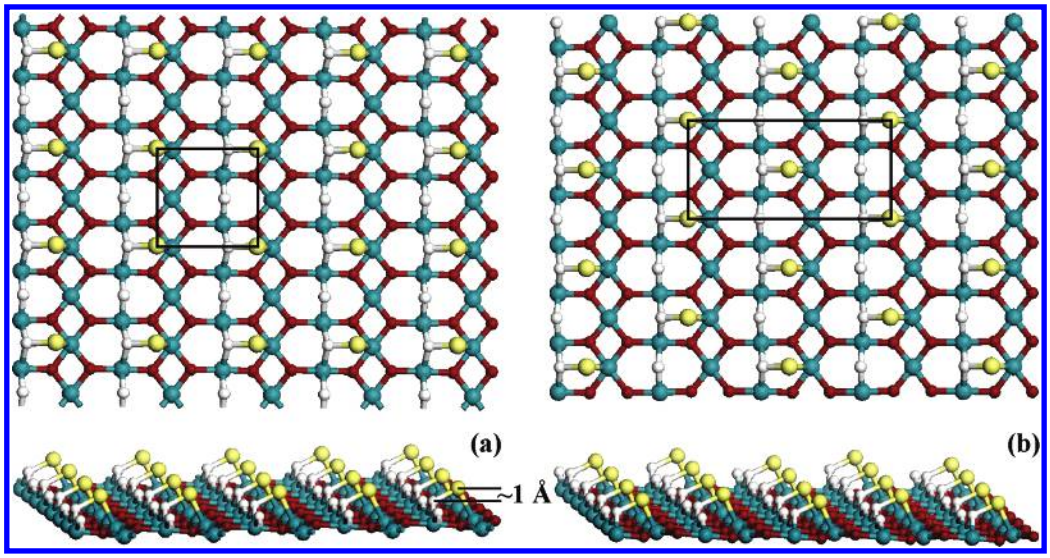

Figure 11. Two possible optimized geometries for 0.25 ML Pt coverage on RuO_2(110) in perspective and side view: (a) 2 × 1 (6.234 Å × 6.442 Å) and (b) c(2 × 2) (6.234 Å × 12.884 Å).

on a 4 × 4 × 1 Monkhorst−Pack *k*-point grid.[23] Increasing the cutoff and the number of *k*-points had no significant effect on the results. For details of the calculations, see ref 19.

The results revealed that the Pt atoms strongly adsorb on RuO_2 and that two-dimensional growth up to 1.25 ML deposition was energetically favorable. At low coverage, the binding between Pt and RuO_2 is very strong, accompanied by a significant transfer of electron density from Pt to the support and a large downshift of the d-band compared to that of the unsupported Pt. At high coverage, a weak interaction of RuO_2 with the Pt cluster is observed, and the electronic structure of Pt is only slightly modified with respect to that of the unsupported material. The prediction of the DFT calculation that Pt atoms strongly adsorb on RuO_2 is not in accord with experimental observation that there is a large overpotential for Pt deposition on RuO_2. The likely reason for this difference is that in the DFT calculation Pt was deposited under UHV conditions, whereas in experiment Pt was deposited under electrochemical conditions.

Comparison of the atomically resolved ECSTM image of the oxide stripe after Pt deposition, Figure 10a, with possible arrangements of Pt atoms at different Pt coverages predicted by DFT calculations[19] suggests that the image is equivalent to the calculated adlayer of 0.25 ML Pt coverage (Pt coverage was calculated in relation to Ru atoms). But why is only a 0.25 ML Pt coverage observed? Figure 12 displays changes of energies with coverage for Pt adsorption on RuO_2(110), viz., the adsorption energy of a free Pt atom on the RuO_2(110) surface (E_{ads}), formation energy of *n* free Pt atoms to an unsupported Pt_n cluster (E_{form}), and desorption energy (E_{des}) which corresponds to the energy cost to desorb a Pt_n cluster from the RuO_2(110) surface. All three energies have a strong dependence on the coverage. Since DFT calculations were done for 0 K, but the data presented were obtained at room temperature, one could expect some difference caused by the deposition conditions. DFT calculations show that at 0.25 ML Pt coverages of RuO_2 there are two possible Pt atom arrangements, 2 × 1 (6.234 Å × 6.442 Å) and c(2 × 2) (6.234 Å × 12.884 Å), and they are related and almost equally probable (only 0.1 eV difference), Figure 11, parts a and b. One is transformed into the other by translating every other row of Pt atoms along the [001] direction for one lattice unit (3.11 Å). ECSTM shows that only the c(2 × 2) array is observed and that, within the limits of accuracy,

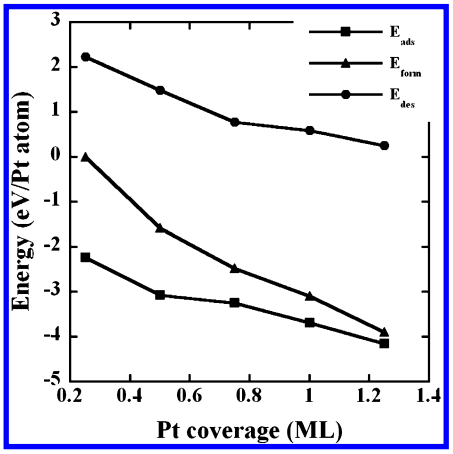

Figure 12. Calculated E_{ads}, E_{form}, and E_{des} energies for the Pt/RuO_2 interface at different Pt coverages.

it agrees with the calculated one. Also, DFT calculations show that Pt atoms lie ~1 Å above the plane of bridging O. This prediction is easy to understand. Pt atoms cannot lie in the plane of Ru atoms because the Pt−Ru distance would be too short, making such configurations energetically unfavorable. Thus, assuming that ECSTM image contrast is governed by geometric effects, as in the case of imaging of RuO_2(110), one could expect to see an ECSTM image like the one depicted in Figure 10a. The small mounds observed in Figure 10b appear to be nuclei of Pt islands. Thus, Figure 10 shows the growth of Pt islands, and from them a three-dimensional Pt deposit, which implies the Stranski−Krastanov growth mode.

3.5. Oxygen Reduction Reaction on Pt onto RuO_2(110). Figure 13 shows the ORR on RuO_2(110), a Pt adlayer on RuO_2(110), and Pt(111) stationary electrodes. The cathodic potential limit for the RuO_2(110) and Pt adlayer on RuO_2(110) is set positive to the limiting potential below which formation of metallic Ru sites and surface roughening appears as discussed in ref 24. The polarization curve for RuO_2(110) shows that it is quite inactive for the ORR. In order to compare the activity for ORR of Pt adlayers on RuO_2(110) and Pt(111), one should take into account that there are 6 times more Pt atoms on a Pt(111) surface than in the Pt adlayer on RuO_2(110) (see Figure 10a and Figure 11b). Thus, the current for the Pt/RuO_2(110) surface is obtained by normalizing the measured current by the Pt(111) coverage. Figure 13 shows that the potential for ORR on a Pt

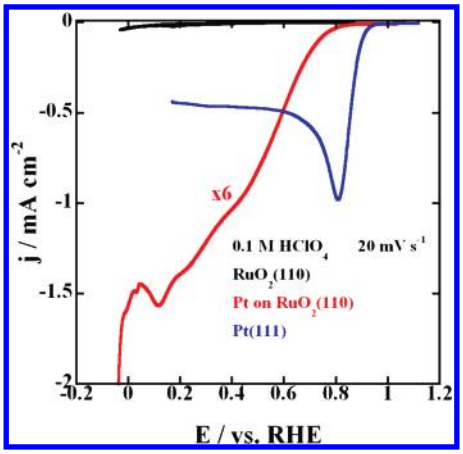

Figure 13. Polarization curves for ORR on RuO_2(110), Pt on RuO_2-(110) normalized by Pt coverage, and Pt(111) stationary electrodes in oxygenated 100 mM $HClO_4$.

adlayer on RuO_2(110) is shifted negatively compared to Pt(111). This shift and smaller kinetic current suggest that the ORR on a Pt adlayer on RuO_2(110) is affected by electronic effects. The lower activity of Pt on RuO_2 compared to Pt(111) could be expected on the basis of a very large upshift of the d-band center of the Pt adlayer on RuO_2(110).[19] Therefore, the supported Pt is too active to catalyze the ORR since it reacts with H_2O and is probably oxidized to Pt−OH, which blocks the ORR. An additional cause of such activity could come from the fact that Pt atoms in the Pt adlayer are fairly distant from each other compared to the Pt−Pt interatomic distance in Pt(111). This might influence the O_2 bonding and orientation toward the Pt adlayer. For this surface there is no possibility for bonding of O_2 with two Pt atoms (bridge model—Yeager[1]), but O_2 can only bond to a single Pt atom with two bonds (Griffith model[1]) or in an end-on adsorption through a single bond (Pauling model[1]). Such an orientation of O_2 molecules is not conducive to the splitting of the O−O bond, thus resulting in a modest activity of such a surface for the ORR. One could argue that the O_2 molecule can bridge between a Pt atom and a Ru atom from the Ru plane and in that way achieve a bridging configuration. Although possible it does not appear to improve the activity if operative. A possible reason for this is that the presence of an oxygen-containing species at a RuO_2 surface in a broad potential range will interfere with the ORR.

4. Conclusions

The electrodeposition of Pt on RuO_2(110) was studied by programmed potential pulses or potential sweeps from several Pt complexes in acid solutions. Electrochemical experiments showed that Pt deposition involves large crystallization overpotential which is likely due to the mismatch between the RuO_2(110) and Pt lattices. The process starts with the deposition of a 0.25 ML of Pt, with Pt atoms arranged in a c(2 × 2) array, which is followed by Pt islands growth and three-dimensional cluster formation. This suggests the Stranski−Krastanov growth mode. The three-dimensional growth is expected since Pt has larger surface energy than RuO_2. Three different kinds of multilayer deposits were observed as a function of the deposition conditions: rectangular, pyramidal, and columnar. Large deposits grow along two orthogonal directions of RuO_2. The three-dimensional deposit consists of Pt islands 2−3 nm in diameter. The deposition process, however, is not uniform over the whole electrode surface. The nucleation is instantaneous, as inferred from the potential step experiments.

DFT calculations were performed to gain additional insights into the atomically resolved ECSTM images of initial stages of Pt deposition onto RuO_2, as well as activity for ORR. It is shown that Pt adlayer on RuO_2(110) has lower catalytic activity for ORR compared to Pt, which is in agreement with a large calculated upshift of the d-band center, as well as a lack of the oxygen adsorption in a bridge configuration on that surface.

The system offers an interesting possibility to study the catalytic reactions on supported single Pt atoms, which will be reported in the near future.

Acknowledgment. This work is supported by U.S. Department of Energy, Divisions of Chemical and Material Sciences, under the Contract No. DE-AC02-98CH10886.

References and Notes

(1) Adzic, R. R. In *Frontiers in Electrochemistry: Electrocatalysis*; Lipkowski, J., Ross, P. N., Eds.; VCH Publishers: New York, 1998; p 197.
(2) Adzic, R. R.; Markovic, N. M. *Electrochim. Acta* **1985**, *30*, 1473.
(3) Ryden, W. D.; Lawson, A. W.; Sartain, C. C. *Phys. Lett.* **1968**, *26A*, 209.
(4) de Almeida, J. S.; Ahuja, R. *Phys. Rev. B* **2006**, *73*, 165102.
(5) Hepel, T.; Pollak, F. H.; O'Grady, W. E. *J. Electroanal. Chem.* **1987**, *236*, 295.
(6) Hepel, T.; Pollak, F. H.; O'Grady, W. E. *J. Electrochem. Soc.* **1988**, *135*, 562.
(7) Vukmirovic, M. B.; Sabatini, R. L.; Adzic, R. R. *Surf. Sci.* **2004**, *572*, 269.
(8) Atanasoska, Lj.; O'Grady, W. E.; Atanasoski, R. T.; Pollak, F. H. *Surf. Sci.* **1988**, *202*, 142.
(9) Over, H.; Kim, Y. D.; Seitsonen, A. P.; Wendt, S.; Lundgren, E.; Schmid, M.; Varga, P.; Morgante, A.; Ertl, G. *Science* **2000**, *287*, 1474.
(10) Over, H.; Seitsonen, A. P.; Lundgren, E.; Schmid, M.; Varga, P. *Surf. Sci.* **2002**, *515*, 143.
(11) Hepel, T.; Pollak, F. H.; O'Grady, W. E. *J. Electrochem. Soc.* **1984**, *131*, 2094.
(12) Lister, T. E.; Chu, Y.; Cullen, W.; You, H.; Yonco, R. M.; Mitchell, J. F.; Nagy, Z. *J. Electroanal. Chem.* **2002**, *524−525*, 201.
(13) Guerrini, E.; Consonni, V.; Trasatti, S. *J. Solid State Electrochem.* **2005**, *9*, 320.
(14) Hepel, T.; Pollak, F. H.; O'Grady, W. E. *J. Electrochem. Soc.* **1986**, *133*, 69.
(15) Galizzioli, D.; Tantardini, F.; Trasatti, S. *J. Appl. Electrochem.* **1974**, *4*, 57.
(16) Mezey, L. Z.; Giber, J. *Jpn. J. Appl. Phys.* **1982**, *21*, 1569.
(17) Kim, Y. D.; Schwegmann, S.; Seitsonen, A. P.; Over, H. *J. Phys. Chem. B* **2001**, *105*, 2205.
(18) Scharifker, B.; Hills, G. *Electrochim. Acta* **1983**, *28*, 879.
(19) Liu, P.; Muckerman, J. T.; Adzic, R. R. *J. Chem. Phys.* **2006**, *124*, 141101.
(20) Payne, M. C.; Allan, D. C.; Arias, T. A.; Johannopoulus, J. D. *Rev. Mod. Phys.* **1992**, *64*, 1045.
(21) Vanderbilt, D. *Phys. Rev. B* **1990**, *41*, 7892.
(22) Hammer, B.; Hansen, L. B.; Nørskov, J. K. *Phys. Rev. B* **1999**, *59*, 7413.
(23) Monkhorst, H. J.; Pack, J. D. *Phys. Rev. B* **1976**, *12*, 5188.
(24) Lister, T. E.; Tolmachev, Y. V.; Chu, Y.; Cullen, W. G.; You, H.; Yonco, R.; Nagy, Z. *J. Electroanal. Chem.* **2003**, *554−555*, 71.